

Mode splitting induced by an arbitrarily shaped Rayleigh scatterer in a whispering-gallery microcavity

Yinglun Xu,¹ Shui-Jing Tang,^{1,2,3} Xiao-Chong Yu,^{1,2} You-Ling Chen,^{4,*}
Daquan Yang,⁵ Qihuang Gong,^{1,2,3} and Yun-Feng Xiao^{1,2,3,†}

¹State Key Laboratory for Mesoscopic Physics and School of Physics, Peking University, Beijing 100871, People's Republic of China

²Collaborative Innovation Center of Quantum Matter, Beijing 100871, People's Republic of China

³Collaborative Innovation Center of Extreme Optics, Shanxi University, Taiyuan 030006, Shanxi, People's Republic of China

⁴State Key Laboratory on Integrated Optoelectronics, Institute of Semiconductors, Chinese Academy of Sciences, Beijing 100083, China

⁵State Key Laboratory of Information Photonics and Optical Communications, School of Information and Communication Engineering, Beijing University of Posts and Telecommunications, Beijing 100876, China



(Received 26 February 2018; revised manuscript received 27 April 2018; published 13 June 2018)

We investigate theoretically the mode splitting induced by an arbitrarily shaped Rayleigh scatterer attached to a whispering-gallery microcavity. The information including polar position, orientation, and polarizability tensor of the nanoparticle can be obtained through the mode-splitting signal. It is found that when the electric field of a pair of counterpropagating modes have different orientations and are not linearly polarized, both of the split modes experience frequency shift and linewidth broadening. The polar angle, at which a nanoparticle binds on the microsphere cavity, can be extracted by comparing frequency splittings of two fundamental TE modes. Moreover, the orientation and polarizability of the particle can be acquired by combining frequency splittings and linewidth broadenings of three modes which polarize the particle in different orientations. This work provides a comprehensive theory base for microcavity sensing of nanoparticles of arbitrary shape instead of nanospheres and could push nanoparticle detection towards quantitative characterization.

DOI: [10.1103/PhysRevA.97.063828](https://doi.org/10.1103/PhysRevA.97.063828)

I. INTRODUCTION

The development of nanoscopic particle detections and characterizations have attracted great attention because of its valuable applications in various fields, such as environmental monitoring, semiconductor manufacturing, and medical diagnostics [1–6]. Recently, whispering-gallery-mode (WGM) microcavities have been demonstrated as powerful platforms to detect and characterize unlabeled nanoparticles [7–20], due to its high quality (Q) factors and small mode volumes. The reactive sensing mechanism is widely applied in nanoparticle detection based on WGM microcavities. In this mechanism, the scattering of a nanoparticle induces the coupling between the clockwise (c) and counterclockwise (cc) propagating modes, resulting in a splitting of cavity modes which is known as mode splitting [21–26]. In addition, when the mode splitting is smaller than the mode linewidth, the splitting cannot be resolved and the transmission behaves as mode shift [27] and mode broadening [28–30]. So far, the detection of individual Influenza A (InfA) can be achieved by monitoring the resonance-wavelength shift [31]. Additionally, through the mode splitting of a WGM Raman microlaser, a single nanoparticle with radius down to 10 nm can be detected [22]. Moreover, via plasmonic enhancement, the detection of single-molecule nucleic acid [29] and single atomic ions have also been demonstrated [30]. However, although label-free

single-nanoparticle detection with ultrasmall size have been demonstrated based on WGM cavities, it is still a challenge for further acquiring more quantitative information on the nanoparticle, such as the size and position.

To break these limitations, a few methods have been developed to obtain the size or the position information of spherical nanoparticles [24,32–35]. However, the limitation on spherical shape hinders their applications in biological study because most kinds of biomolecules are geometrically anisotropic. In addition, some works have investigated the case of anisotropic nanoparticles adsorbed by a microcavity [36–38]. For example, Arnold *et al.* proposed and experimentally demonstrated that the ratio of the mode shift of TM and TE mode is sensitive to the shape and orientation of anisotropic nanoparticles [36,37], yet they did not realize quantitative measurements. Furthermore, Yi *et al.* proposed theoretically a method to acquire the orientation of a single cylinder-shaped nanoparticle [38]. However, there is no progress on obtaining quantitative information such as the position and polarizability tensor of the nanoparticle.

In this paper, we utilize mode splitting to acquire the position, orientation, and polarizability tensor of a single arbitrarily shaped Rayleigh nanoparticle using a WGM microcavity. Under the dipole approximation, we theoretically investigate the mode splitting induced by an arbitrary-shaped particle coupled to a WGM microcavity. It is found that the degeneracy of a pair of counterpropagating modes, of which the electric fields have the same orientation and are linearly polarized, are lifted by the particle. As a result, one mode experiences frequency shift and linewidth broadening, while

*ylchen@semi.ac.cn

†yfxiao@pku.edu.cn; <http://www.phy.pku.edu.cn/~yfxiao/>

the other remains unchanged, as proposed by the pioneering work of Ref. [21]. However, when the electric field of a pair of counterpropagating modes have different orientations or are not linearly polarized, both of the split modes experience frequency shift and linewidth broadening. Furthermore, some previous theories [24,33,34] for characterizing spherical nanoparticles, which are based on the fact that the coupling strength and the damping rate share the same polarizability in this special case, cannot be applied to characterize anisotropic nanoparticles. For anisotropic particles, the effective polarizabilities (equivalent to the polarizability of a sphere particle) in the coupling strength between modes are different from that in the damping rate of modes under different polarization orientations. Here, the polar position of an anisotropic particle binding on the microcavity can be extracted by comparing the frequency splittings of two fundamental TE modes of a microsphere cavity. Then, the orientation and polarizability of the nanoparticle can be acquired through three modes which polarize the nanoparticle in different orientations, e.g., two fundamental TM modes and one fundamental TE mode of a microsphere cavity.

This paper is organized as follows: In Sec. II, we analyze the scattering of an arbitrarily shaped particle coupled to a WGM microcavity. The physical origin of mode splitting is explained. In Sec. III, the position of the particle is obtained based on mode splitting. In Sec. IV, the orientation and polarizability tensor of the particle are acquired. In Sec. V, we study the detection limit of a special kind of anisotropic nanoparticles, the ellipsoid nanoparticles. Finally, a summary is presented.

II. MODE SPLITTING INDUCED BY A SINGLE ANISOTROPIC PARTICLE

The schematic of the interaction between WGMs and an anisotropic nanoparticle is plotted in Fig. 1(a). Here, the nanoparticle is a nonabsorbing Rayleigh scatterer; that is, the scale of the particle is subwavelength. The evanescent field of a tapered fiber can be coupled to the WGMs of the microcavity [39,40], and the transmission spectrum is used to characterize the mode structures (i.e., the resonance frequency and the linewidth) [35,41,42]. The particle within the mode field acts as a scatterer and couples to a pair of counterpropagating modes. The scattering of the particle induces the coupling between modes with strength g , and the coupling of modes to the reservoir with damping rate Γ . The interaction lifts the mode degeneracy and leads to mode splitting.

The mechanisms of the mode splitting can be modeled within the dipole approximation [21]. The electric field \mathbf{E} of one traveling mode, i.e., clockwise (c) traveling mode or counterclockwise (cc) traveling mode, induces a dipole moment $\mathbf{P}_{c(cc)} \propto -\vec{\alpha} \cdot \mathbf{E}_{c(cc)}$ in the particle, where $\vec{\alpha}$ is the polarizability of the anisotropic particle. Then the dipole \mathbf{P}_i interacts with the traveling mode \mathbf{E}_i and the opposite traveling mode \mathbf{E}_j , which introduces coupling between the two traveling modes with strength $g_{i,j} \propto \mathbf{P}_i^* \cdot \mathbf{E}_j - (\vec{\alpha} \cdot \mathbf{E}_i)^* \cdot \mathbf{E}_j$, where i, j represent c or cc. The dipole also couples to the reservoir and opens a loss channel with damping rate $\Gamma_{c(cc)} \propto |\sum_j \mathbf{P}_{c(cc)}^* \cdot \mathbf{E}_r|^2 \propto |\sum_j (\vec{\alpha} \cdot \mathbf{E}_{c(cc)})^* \cdot \mathbf{E}_r|^2$, where \mathbf{E}_r denotes the electric field of reservoir modes. When the electric fields of the two traveling modes are linearly polarized and have the same

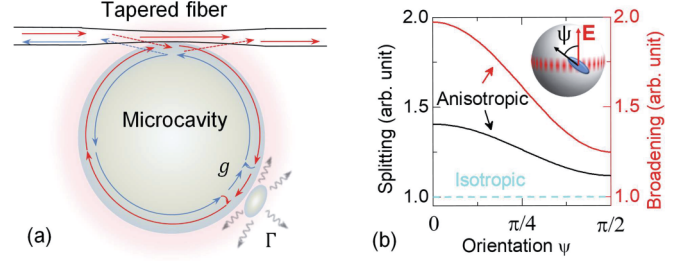


FIG. 1. (a) Schematic diagram of an anisotropic nanoparticle coupled to a WGM microcavity. The scattering of the particle induces the coupling between the counterpropagating modes with the strength g , and the coupling of modes to the reservoir with the damping rate Γ . (b) The detection signal of anisotropic and isotropic nanoparticles for a TE mode of a microsphere cavity, as a function of the orientation Ψ of the particle. Here, the anisotropic particle is an ellipsoid with three semimajor axes of length (9, 3, 1). The orientation Ψ is the angle between the orientation of electric field and the longest semimajor axis of the ellipsoid, and the shortest semimajor axis of the ellipsoid is vertical to the cavity (Inset). The frequency splitting and the linewidth broadening induced by an isotropic particle are not relevant to the orientation Ψ of particle, which are denoted by the blue dashed curve. The frequency splitting (black solid curve) and the linewidth broadening (red solid curve) induced by an anisotropic particle are normalized by those induced by an isotropic particle with the same volume.

orientation, the four coupling strengths are equal $g_{i,j} = g_{i',j'}$, and the two damping rates comply $\Gamma_c = \Gamma_{cc}$, as proposed by a pioneering work Ref. [21]. Otherwise, the four coupling strengths and the two damping rates are different ($g_{i,j} \neq g_{i',j'}$, $\Gamma_c \neq \Gamma_{cc}$). Here we take the mode splittings of TE modes and TM modes of a microsphere cavity as examples to discuss the mode splitting in these two situations.

A. Mode splitting of TE modes

The electric fields of a pair of counterpropagating TE modes of a microsphere cavity can be approximated as linearly polarized, and their orientations are the same. The four coupling strengths and the two damping rates are equal, respectively denoted as g and Γ . Induced by the scattering of the particle, the two degenerate counterpropagating modes split into two nondegenerate modes. One mode remains unchanged while the other mode experiences a frequency redshift of $-2g$, and linewidth broadening of Γ . Here, based on Ref. [21], g and Γ are written as

$$g = -\frac{f^2(\xi)}{2V_c} \alpha_{\text{eff}}^{(1)} \omega, \quad (1)$$

$$\Gamma = \frac{f^2(\xi)}{V_c} |\alpha_{\text{eff}}^{(2)}|^2 \frac{\omega^4}{6\pi c^3}, \quad (2)$$

where ω is the resonant frequency, c is the speed of light in the medium surrounding the cavity, ξ is the polar position of the particle, and $f(\xi)$ is the mode distribution of the WGM at the polar position ξ on the surface of the microsphere cavity. The mode volume V_c is defined as

$$V_c = \frac{\int_V \epsilon(\mathbf{r}) |\mathbf{E}(\mathbf{r})|^2 d^3\mathbf{r}}{\max[\epsilon(\mathbf{r}) |\mathbf{E}(\mathbf{r})|^2]},$$

where $\epsilon(\mathbf{r})$ and $\mathbf{E}(\mathbf{r})$ are the dielectric constant of the material and the electric field at the position \mathbf{r} . It should be noted that the azimuthal position only affects the phase of the electric field of traveling modes for a spherical symmetric microcavity, and the phase of electric field has no effect on g or Γ induced by a single adsorbed nanoparticle. Therefore, the azimuthal position of the particle does not affect g or Γ . From the physical origin of g and Γ discussed above, we can find that the effective polarizabilities $\alpha_{\text{eff}}^{(1)}$ and $\alpha_{\text{eff}}^{(2)}$ are different. Through calculation, $\alpha_{\text{eff}}^{(1)}$ and $\alpha_{\text{eff}}^{(2)}$ can be written as

$$\alpha_{\text{eff}}^{(1)} = [\vec{\alpha} \cdot \mathbf{n}(\xi)]^\dagger \cdot \mathbf{n}(\xi), \quad (3)$$

$$\alpha_{\text{eff}}^{(2)} = |\vec{\alpha} \cdot \mathbf{n}(\xi)|, \quad (4)$$

where $\mathbf{n}(\xi)$ is the unit vector of the electric field at the polar position ξ .

B. Mode splitting of TM modes

The electric fields of a pair of counterpropagating TM modes of a microsphere cavity are elliptically polarized, i.e., $\mathbf{n}(\xi)$ contains complex elements, and their orientations are different. For TM modes, the coupling strengths $g_{c,c}$, $g_{cc,cc}$, $g_{c,cc}$, $g_{cc,c}$, and the two damping rates Γ_c , Γ_{cc} are

$$g_{i,j} = -\frac{f^2(\xi)}{2V_c} \alpha_{\text{eff}}^{ij(1)} \omega, \quad (5)$$

$$\Gamma_i = \frac{f^2(\xi)}{V_c} |\alpha_{\text{eff}}^{i(2)}|^2 \frac{\omega^4}{6\pi c^3}, \quad (6)$$

where i, j represent c and cc . The effective polarizabilities $\alpha_{\text{eff}}^{ij(1)}$ and $\alpha_{\text{eff}}^{i(2)}$ are

$$\alpha_{\text{eff}}^{ij(1)} = [\vec{\alpha} \cdot \mathbf{n}_i(\xi)]^\dagger \cdot \mathbf{n}_j(\xi), \quad (7)$$

$$\alpha_{\text{eff}}^{i(2)} = |\vec{\alpha} \cdot \mathbf{n}_i(\xi)|. \quad (8)$$

The coupling function between the two counterpropagating modes [21] are written as

$$\frac{d}{dt} \begin{pmatrix} a_c \\ a_{cc} \end{pmatrix} = \begin{bmatrix} -(ig_{c,c} + \frac{1}{2}\Gamma_c) & -(ig_{cc,c} + \frac{1}{2}\Gamma_{cc}) \\ -(ig_{c,cc} + \frac{1}{2}\Gamma_c) & -(ig_{cc,cc} + \frac{1}{2}\Gamma_{cc}) \end{bmatrix} \begin{pmatrix} a_c \\ a_{cc} \end{pmatrix}. \quad (9)$$

Here, a_c and a_{cc} are annihilation operators of the electric fields of the modes. The frequency shifts and the linewidth broadening of the two new eigenmodes can be acquired by deriving the eigenvalue of the coupling matrix. As a result, for the mode splitting of TM modes of a microsphere cavity, both of the two split modes experience frequency shifts and linewidth broadenings. The sum of frequency shifts of two modes equals $-g_{c,c} - g_{cc,cc} \triangleq -2\bar{g}$, and the sum of linewidth broadening equals $(\Gamma_c + \Gamma_{cc})/2 \triangleq \bar{\Gamma}$. Here, \bar{g} and $\bar{\Gamma}$ are

$$\bar{g} = -\frac{f^2(\xi)}{2V_c} \bar{\alpha}_{\text{eff}}^{(1)} \omega, \quad (10)$$

$$\bar{\Gamma} = \frac{f^2(\xi)}{V_c} |\bar{\alpha}_{\text{eff}}^{(2)}|^2 \frac{\omega^4}{6\pi c^3}, \quad (11)$$

where $\bar{\alpha}_{\text{eff}}^{(1)}$ and $\bar{\alpha}_{\text{eff}}^{(2)}$ are written as

$$\bar{\alpha}_{\text{eff}}^{(1)} = \frac{1}{2} \{ [\vec{\alpha} \cdot \mathbf{n}_c(\xi)]^\dagger \cdot \mathbf{n}_c(\xi) + [\vec{\alpha} \cdot \mathbf{n}_{cc}(\xi)]^\dagger \cdot \mathbf{n}_{cc}(\xi) \}, \quad (12)$$

$$|\bar{\alpha}_{\text{eff}}^{(2)}|^2 = \frac{1}{2} [|\vec{\alpha} \cdot \mathbf{n}_c(\xi)|^2 + |\vec{\alpha} \cdot \mathbf{n}_{cc}(\xi)|^2], \quad (13)$$

where $\mathbf{n}_c(\xi)$ and $\mathbf{n}_{cc}(\xi)$ are the unit vector of the electric field of the two traveling TM modes, respectively. In the following discussion, we use $|2g|$ ($|2\bar{g}|$) and Γ ($\bar{\Gamma}$) as the detection signals. It should be noticed that, for TM modes, $|2\bar{g}|$ and $\bar{\Gamma}$ are acquired by the sum of frequency shifts and linewidth broadenings of two split modes, respectively. While for TE modes, $|2g|$ and Γ are acquired by the frequency splitting of the two split modes and the linewidth broadening of the broadened split mode.

As an example of an anisotropic particle, we take a polystyrene (refractive index $n = 1.59$) nano-ellipsoid with three semimajor axes of length (9, 3, 1) in air. The corresponding three principle polarizabilities, normalized by the polarizability of a nanosphere with the same volume and material, is (1.40, 1.12, 0.72). The method to derive the principle polarizability from the geometrical factor of an ellipsoid can be found in Ref. [43]. For a conventional situation where the particle is polarized by a TE mode, the frequency splitting and linewidth broadening are calculated under different particle orientations Ψ , as shown in Fig. 1(b). As Ψ varies from 0 to $\pi/2$, the frequency splitting and the linewidth broadening induced by an anisotropic particle decreases, which is distinctly different from that of isotropic particles.

To demonstrate the impact of the geometry factor of the nanoparticle on mode splitting, the ratio between $\alpha_{\text{eff}}^{(1)}$ and $\alpha_{\text{eff}}^{(2)}$ for a particle of arbitrary shape is depicted in Fig. 2. As an example, we choose a particle of which the normalized three principle polarizabilities are $(\alpha_x, \alpha_y, \alpha_z) = (10, 3, 1)$, representing a long and thin particle. The configuration of the interaction between the particle and the microcavity is the same as Fig. 1(a). In Figs. 2(a)–2(c), we show a special case where a particle lies on a cavity with one principle axis vertical to the cavity and the other two rotating in the tangential plane. The orientation of the electric field is represented by polar and azimuthal angles in the coordinate based on the polarizability tensor, as shown in the insets of the Fig. 2(a)–2(c). In general, Fig. 2(d) shows the ratio between $\alpha_{\text{eff}}^{(1)}$ and $\alpha_{\text{eff}}^{(2)}$ under all polarization orientations. It shows that the ratio of $\alpha_{\text{eff}}^{(1)}$ and $\alpha_{\text{eff}}^{(2)}$ relies on the orientation of the electric field, and $\alpha_{\text{eff}}^{(1)} = \alpha_{\text{eff}}^{(2)}$ only when the orientation of the electric field is parallel to one of the principle axis of the particle's polarizability matrix.

III. POLAR POSITION OF AN ANISOTROPIC PARTICLE

Here we discuss the mechanism to acquire the polar position of an anisotropic particle on the cavity. For a nanosphere, its polarizability can be acquired by dividing the linewidth broadening Γ by the frequency splitting $|2g|$, as pointed out by some previous works [24,38], and then the position of the particle can be obtained. However, owing to the difference between the two effective polarizabilities in g and Γ , the previous methods are no longer suitable for anisotropic nanoparticles.

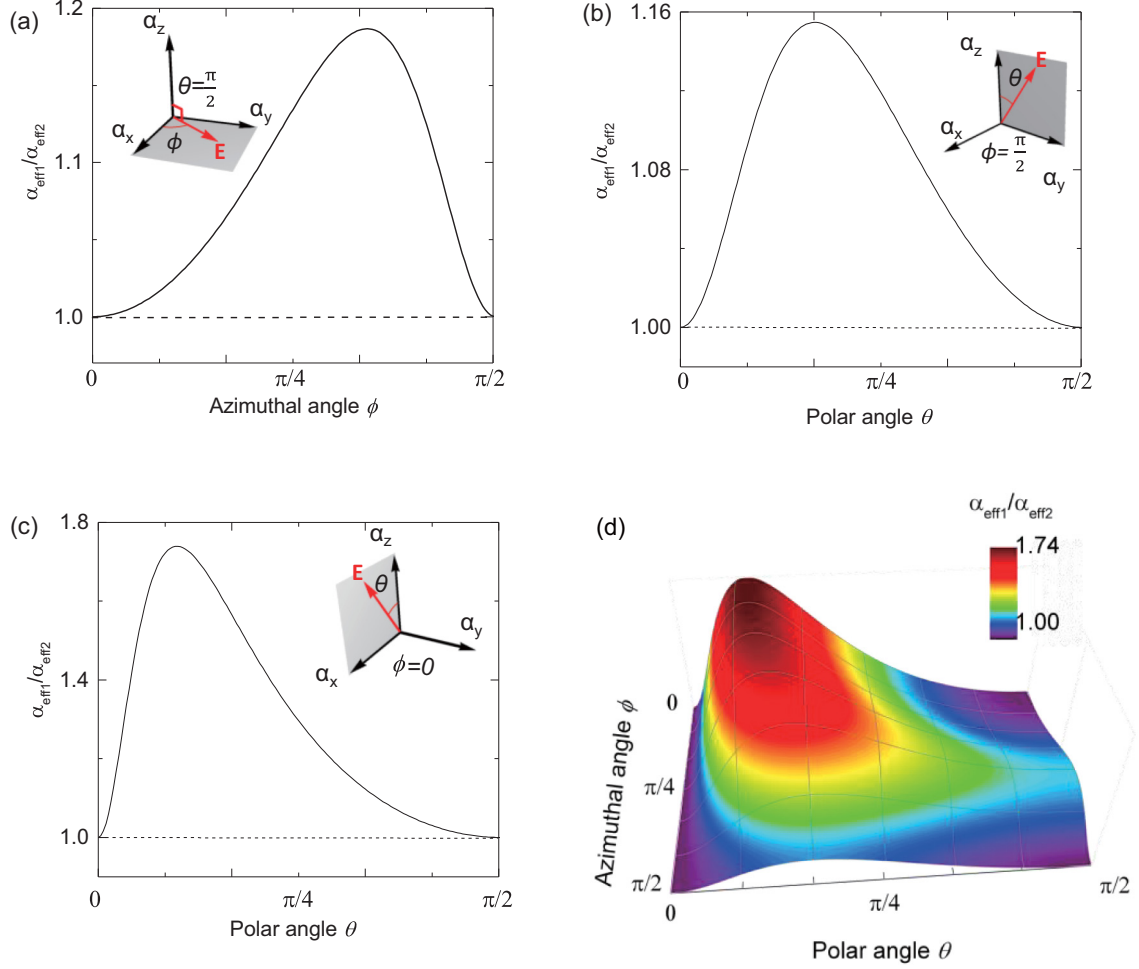


FIG. 2. Ratio between the two effective polarizabilities of frequency splitting and linewidth broadening for an anisotropic nanoparticle as a function of the orientation of the TE electric field \mathbf{E} of a microsphere cavity. The orientation of the electric field rotates in the (a) α_x - α_y , (b) α_y - α_z , and (c) α_x - α_z planes. (d) The orientation of the electric field is arbitrary. The insets show the orientation of the electric field \mathbf{E} . The three coordinate axes are parallel to the three principle axes of the polarizability tensor of the particle. The polar angle θ and the azimuthal angle ϕ are used to represent the orientation of the electric field \mathbf{E} . Here, the three principle polarizabilities of the particle are taken as (10, 3, 1).

Here, the position of an anisotropic particle can be obtained by the ratio of frequency splitting $|2g|$ of two fundamental TE modes of a microsphere cavity, of which the electric fields have almost the same orientation. It is obvious that the effective polarizability $\alpha_{\text{eff}}^{(1)}$ of the particle for these two modes are the same, because the particle is polarized by the electric fields with the same orientation. According to Eq. (1), the ratio can be written as

$$\frac{g_{TE_{l,l}}}{g_{TE_{l-1,l-1}}} = \frac{\omega_{l,l}}{\omega_{l-1,l-1}} \frac{f_{TE_{l,l}}^2(\xi)}{f_{TE_{l-1,l-1}}^2(\xi)}, \quad (14)$$

where the expression of $f_{TE}(\xi)$ for a microsphere cavity can be found in Ref. [36]. The polar position of the nanoparticle can be acquired by solving ξ from Eq. (14). It should be noted that there might be multiple ξ that satisfy Eq. (14). If this happens, another pair of fundamental TE modes should be utilized in Eq. (14) to confirm the polar position ξ of the nanoparticle and exclude the disturbance of multiple ξ .

IV. ORIENTATION AND POLARIZABILITY OF AN ANISOTROPIC NANOPARTICLE

Once the polar position of the nanoparticle has been obtained, the polarizability and orientation of the particle can be achieved by using cavity modes with different electric-field orientations.

Through mode splitting of TE modes, we can derive $\alpha_{\text{eff}}^{(1)}$ and $\alpha_{\text{eff}}^{(2)}$ from the frequency separation $|2g|$ and the linewidth broadening Γ by using Eqs. (1) and (2). Under a given Cartesian coordinate, the polarizability $\vec{\alpha}$ of the particle and the electric-field orientation \mathbf{n} of the WGM at the position of the particle can be written as

$$\vec{\alpha} = \begin{bmatrix} \alpha_{xx} & \alpha_{xy} & \alpha_{xz} \\ \alpha_{yx} & \alpha_{yy} & \alpha_{yz} \\ \alpha_{zx} & \alpha_{zy} & \alpha_{zz} \end{bmatrix}, \quad \mathbf{n} = \begin{pmatrix} n_x \\ n_y \\ n_z \end{pmatrix}. \quad (15)$$

The number of independent elements of the polarizability tensor $\vec{\alpha}$ is determined by the particle geometry (1, 4, and 6 for sphere, cylindrical, and anisotropic particle, respectively).

According to Eqs. (3) and (4), the effective polarizabilities can be written as

$$\alpha_{\text{eff}}^{(1)} = \sum_i \alpha_{ii} n_i^2 + \sum_{i,j,i \neq j} 2\alpha_{ij} n_i n_j, \quad (16)$$

$$\alpha_{\text{eff}}^{(2)} = \sqrt{\sum_{i,j,i \neq j} 2(\alpha_{ii} + \alpha_{jj})\alpha_{ij} n_i n_j + \sum_i \sum_j \alpha_{ij}^2 n_i^2}, \quad (17)$$

where i, j represent x, y, z .

For mode splittings of TM modes, the detection signals we use are the sum of frequency shifts $-2\bar{g}$ and linewidth broadening $\bar{\Gamma}$ of two split modes. From these signals, $\bar{\alpha}_{\text{eff}}^{(1)}$ and $\bar{\alpha}_{\text{eff}}^{(2)}$ can be derived by using Eqs. (5) and (6). In this case,

$$\begin{aligned} \bar{\alpha}_{\text{eff}}^{(1)} &= \sum_i \alpha_{ii} \frac{1}{2} (|n_{ci}|^2 + |n_{cci}|^2) \\ &+ \sum_{i,j,i \neq j} \alpha_{ij} \frac{1}{2} [(n_{ci}^* n_{cj} + n_{cci}^* n_{ccj}) + \text{c.c.}], \end{aligned} \quad (18)$$

$$\begin{aligned} \bar{\alpha}_{\text{eff}}^{(2)} &= \left\{ \sum_{i,j,i \neq j} (\alpha_{ii} + \alpha_{jj}) \alpha_{ij} \frac{1}{2} [(n_{ci}^* n_{cj} + n_{cci}^* n_{ccj}) + \text{c.c.}] \right. \\ &\left. + \sum_i \sum_j \alpha_{ij}^2 \frac{1}{2} (|n_{ci}|^2 + |n_{cci}|^2) \right\}^{\frac{1}{2}}, \end{aligned} \quad (19)$$

where n_{ci} and n_{cci} denote components of the unit vectors of the electric field of clockwise and counterclockwise traveling TM modes.

The polar position ξ of the particle can be obtained by using Eq. (14). Combining the mode distribution $f(\xi)$ of a microsphere cavity given in Ref. [36], the unit vector \mathbf{n} of the electric field at position ξ can be obtained. Then, by combining the equations of six effective polarizabilities, which requires three splitting modes with different electric-field orientations at the particle's position ξ (for example, two fundamental TM modes and one fundamental TE mode), all six components of the polarizability tensor $\bar{\alpha}$ can be derived. By diagonalizing the tensor, the polarizability under its principle axis coordinate can be acquired. The corresponding unitary matrix, which diagonalizes the tensor, describes the orientation of the particle binding on the microcavity.

V. DETECTION LIMIT

In the following, we switch to study the detection limit for an arbitrarily shaped particle based on mode splitting. The detection limit is set by the condition that the two split modes should be resolved in the transmission spectra, which requires the frequency splitting $|2g|$ to be greater than the linewidth [7]. The linewidth contains two parts: the intrinsic linewidth of the mode Γ_0 before particle binding and the linewidth broadening upon particle binding. The criteria can be expressed as $|2g| > \Gamma_0 + \Gamma$. The detection limit for nanosphere particles of mode splitting is usually in the range of 10 to 30 nm in radius [22–24] and, for nanoparticles of this size, $|2g| \gg \Gamma$. As a result, the detection limit can be approximated as $|2g| > \Gamma_0$. The geometrical shape of the particle has an important effect on

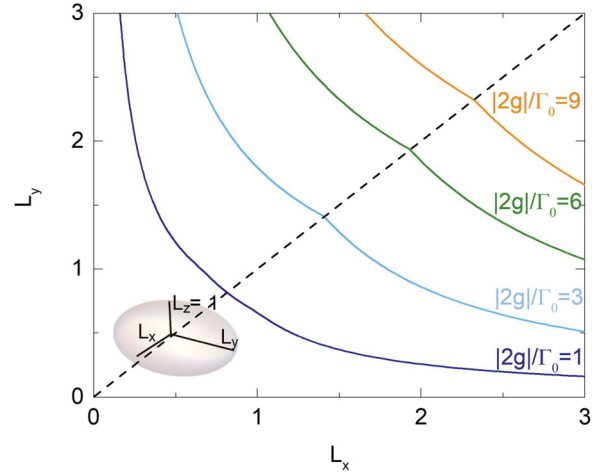


FIG. 3. Ratio of frequency splitting $|2g|$ to intrinsic linewidth Γ_0 for ellipsoid nanoparticles with different geometrical shape factors ($L_x, L_y, L_z = 1$). All curves are symmetric about the angular bisector of the x axis and y axis (the dashed black line). The inset shows that the lengths of three semimajor axes of the nanoparticle are L_x, L_y , and the given $L_z = 1$.

the signals of mode splitting. Here, in Fig. 3, we take ellipsoid particles with geometrical shape factors (length of semimajor axes L_x, L_y , and $L_z = 1$) as an example to discuss the ratio $|2g|/\Gamma_0$ between the frequency splitting $|2g|$ and the intrinsic linewidth of the mode Γ_0 for the arbitrarily shaped nanoparticle binding on the microcavity. Note that the curves shown in Fig. 3 are not hyperbola, which indicates that the volume of the particle is different for same $|2g|/\Gamma_0$. More specifically, the volume for a spherical particle ($L_x = L_y$) is larger than that for a strip-shaped particle ($L_x \gg L_y$ or $L_x \ll L_y$).

As a general example, we discuss the case of ellipsoidal particles in detail. For a given volume of an ellipsoidal particle polarized by TE modes of a microsphere cavity, the maximum signal of frequency splitting under different geometrical shape factors (L_x and L_y) is calculated by utilizing Eq. (1). It shows that, for particles of the same volume, the maximum frequency splitting $|2g|_{\text{max}}$ varies as the shape changes. This quantity decreases for the particle with less eccentric shape. That is, for a fixed volume, $|2g|_{\text{max}}$ reaches a minimum for spherical-shaped particles, while it increases with eccentricity of the particle and approaches the maximum. By calculating $|2g|_{\text{max}}/\Gamma_0$ under different particle volume V and intrinsic linewidth Γ_0 of the cavity mode, the V - Γ_0 space can be divided into three regions, as shown in Fig. 4. In the totally detectable region, $|2g|_{\text{max}}/\Gamma_0 > 1$ holds for any eccentricity; in the undetectable region, $|2g|_{\text{max}}/\Gamma_0 < 1$; in the partially detectable region, the criteria $|2g|_{\text{max}}/\Gamma_0 > 1$ is satisfied for particles with eccentricity large enough. The upper and lower boundaries represent the detection limit of particles with spherical and strip shapes, respectively.

VI. SUMMARY

We theoretically study the mode splitting induced by an arbitrarily shaped nanoparticle in a microcavity. The quantitative information including polar position, polarizability, and

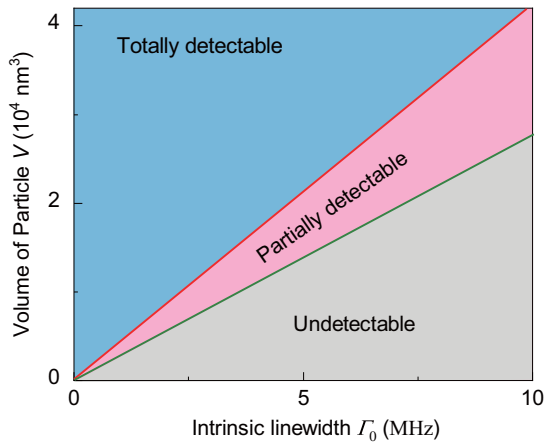


FIG. 4. Detectable region division under different particle volume V and intrinsic linewidth Γ_0 of cavity modes. Blue (purple) regions stand for totally (partially) detectable region where particles with any eccentricity (some eccentricity) in this region can be detected. Gray regions represent undetectable region where no particles in this region can be detected. The red (green) division line represents the detection limit of spherical (strip-shaped) nanoparticles. Here, $f(r) = 0.26$, $V_c = 500 \mu\text{m}$, $\omega = 1.216 \times 10^{15}$ Hz.

orientation of the anisotropic nanoparticle can be acquired. It is found that, for TM modes of a microsphere cavity, both of the split modes experience frequency shifts and linewidth broadenings. The characterization of the polarizability tensor enables us to explore the study of molecular distinction.

The position and the orientation information as well as the real-time-detection nature of WGM microcavities enable us to perform real-time analysis of molecular dynamics.

The nanoparticles we studies are nonabsorbing Rayleigh scatterers. The reactive sensing mechanism based on the dipole approximation is appropriate for this kind of nanoparticle. However, for an absorbing nanoparticle such as a metal nanoparticle binding on the microcavity, its polarizability has a nonzero imaginary part. In this case, the dissipative sensing principle instead of the reactive sensing principle should be used. Our theory can be extended to characterize the dissipative nanoscale objects by modifying the expressions of frequency splitting and linewidth broadening. For a large nanoparticles, the dipole approximation no longer applies [44–47] and more modes need to be selected to acquire the properties of the nanoparticle. Furthermore, combined with the mechanism in Refs. [26,48], our theory has the potential to provide information of each nanoparticle when particles are sequentially adsorbed by the cavity.

ACKNOWLEDGMENTS

We thank Qi-Tao Cao, Yanyan Zhi and Li Wang for their helpful discussion. This work was supported by the NSFC (Grants No. 61435001, No. 11704375, No. 61611540346, No. 11474011, and No. 11654003), the National Key R&D Program of China (Grant No. 2016YFA0301302), and High-performance Computing Platform of Peking University. Y. Xu was supported by the National Fund for Fostering Talents of Basic Science (Grant No. 7310200622).

Y. Xu and S.-J. Tang contributed equally to this work.

-
- [1] J. N. Anker, W. P. Hall, O. Lyandres, N. C. Shah, J. Zhao, and R. P. Van Duyne, *Nat. Mater.* **7**, 442 (2008).
 - [2] X. Fan, I. M. White, S. I. Shopova, H. Zhu, J. D. Suter, and Y. Sun, *Anal. Chim. Acta* **620**, 8 (2008).
 - [3] X.-C. Yu, B.-B. Li, P. Wang, L. Tong, X.-F. Jiang, Y. Li, Q. Gong, and Y.-F. Xiao, *Adv. Mater.* **26**, 7462 (2014).
 - [4] D. Yang, F. Gao, Q.-T. Cao, C. Wang, Y. Ji, and Y.-F. Xiao, *Photonics Res.* **6**, 99 (2018).
 - [5] N. Zhang, S. Liu, K. Wang, Z. Gu, M. Li, N. Yi, S. Xiao, and Q. Song, *Sci. Rep.* **5**, 11912 (2015).
 - [6] C. Wang, Q. Quan, S. Kita, Y. Li, and M. Lončar, *Appl. Phys. Lett.* **106**, 261105 (2015).
 - [7] F. Vollmer and L. Yang, *Nanophotonics* **1**, 267 (2012).
 - [8] Y. Zhi, X.-C. Yu, Q. Gong, L. Yang, and Y.-F. Xiao, *Adv. Mater.* **29** (2017).
 - [9] J. R. Lopez, E. Treasurer, K. M. Snyder, D. Keng, and S. Arnold, *Appl. Phys. Lett.* **112**, 051109 (2018).
 - [10] J. Xavier, S. Vincent, F. Meder, and F. Vollmer, *Nanophotonics* **7**, 1 (2018).
 - [11] J. Su, A. F. Goldberg, and B. M. Stoltz, *Light: Sci. Appl.* **5**, e16001 (2016).
 - [12] K. D. Heylman, N. Thakkar, E. H. Horak, S. C. Quillin, C. Cherqui, K. A. Knapper, D. J. Masiello, and R. H. Goldsmith, *Nat. Photonics* **10**, 788 (2016).
 - [13] L. He, Ş. K. Özdemir, J. Zhu, W. Kim, and L. Yang, *Nat. Nanotechnol.* **6**, 428 (2011).
 - [14] W. Yu, W. C. Jiang, Q. Lin, and T. Lu, *Nat. Commun.* **7**, 12311 (2016).
 - [15] X. Zhang, L. Liu, and L. Xu, *Appl. Phys. Lett.* **104**, 033703 (2014).
 - [16] J. D. Swaim, J. Knittel, and W. P. Bowen, *Appl. Phys. Lett.* **102**, 183106 (2013).
 - [17] Y. Yang, J. Ward, and S. N. Chormaic, *Opt. Express* **22**, 6881 (2014).
 - [18] Y.-L. Chen, W.-L. Jin, Y.-F. Xiao, and X. Zhang, *Phys. Rev. Appl.* **6**, 044021 (2016).
 - [19] J. Su, *ACS Photonics* **2**, 1241 (2015).
 - [20] N. Zhang, Z. Gu, S. Liu, Y. Wang, S. Wang, Z. Duan, W. Sun, Y.-F. Xiao, S. Xiao, and Q. Song, *Optica* **4**, 1151 (2017).
 - [21] A. Mazzei, S. Göttinger, L. de S. Menezes, G. Zumofen, O. Benson, and V. Sandoghdar, *Phys. Rev. Lett.* **99**, 173603 (2007).
 - [22] Ş. K. Özdemir, J. Zhu, X. Yang, B. Peng, H. Yilmaz, L. He, F. Monifi, S. H. Huang, G. L. Long, and L. Yang, *Proc. Natl. Acad. Sci. U. S. A.* **111**, E3836 (2014).
 - [23] B.-B. Li, W. R. Clements, X.-C. Yu, K. Shi, Q. Gong, and Y.-F. Xiao, *Proc. Natl. Acad. Sci. U. S. A.* **111**, 14657 (2014).
 - [24] J. Zhu, S. K. Ozdemir, Y.-F. Xiao, L. Li, L. He, D.-R. Chen, and L. Yang, *Nat. Photonics* **4**, 122 (2010).

- [25] S. Li, L. Ma, S. Böttner, Y. Mei, M. R. Jorgensen, S. Kiravittaya, and O. G. Schmidt, *Phys. Rev. A* **88**, 033833 (2013).
- [26] J. Zhu, Ş. K. Özdemir, L. He, and L. Yang, *Opt. Express* **18**, 23535 (2010).
- [27] L. Shao, X.-F. Jiang, X.-C. Yu, B.-B. Li, W. R. Clements, F. Vollmer, W. Wang, Y.-F. Xiao, and Q. Gong, *Adv. Mater.* **25**, 5616 (2013).
- [28] F. Vollmer, D. Braun, A. Libchaber, M. Khoshima, I. Teraoka, and S. Arnold, *Appl. Phys. Lett.* **80**, 4057 (2002).
- [29] M. D. Baaske, M. R. Foreman, and F. Vollmer, *Nat. Nanotechnol.* **9**, 933 (2014).
- [30] M. D. Baaske and F. Vollmer, *Nat. Photonics* **10**, 733 (2016).
- [31] F. Vollmer, S. Arnold, and D. Keng, *Proc. Natl. Acad. Sci. USA* **105**, 20701 (2008).
- [32] D. Keng, X. Tan, and S. Arnold, *Appl. Phys. Lett.* **105**, 46 (2014).
- [33] W. Kim, S. K. Ozdemir, J. Zhu, F. Monifi, C. Coban, and L. Yang, *Opt. Express* **20**, 29426 (2012).
- [34] J. Zhu, Ş. K. Özdemir, L. He, D.-R. Chen, and L. Yang, *Opt. Express* **19**, 16195 (2011).
- [35] S. Arnold, M. Khoshima, I. Teraoka, S. Holler, and F. Vollmer, *Opt. Lett.* **28**, 272 (2003).
- [36] I. Teraoka and S. Arnold, *J. Opt. Soc. Am. B* **23**, 1381 (2006).
- [37] M. Noto, D. Keng, I. Teraoka, and S. Arnold, *Biophys. J.* **92**, 4466 (2007).
- [38] X. Yi, Y.-F. Xiao, Y. Li, Y.-C. Liu, B.-B. Li, Z.-P. Liu, and Q. Gong, *Appl. Phys. Lett.* **97**, 203705 (2010).
- [39] J. C. Knight, G. Cheung, F. Jacques, and T. Birks, *Opt. Lett.* **22**, 1129 (1997).
- [40] M. Cai, O. Painter, and K. J. Vahala, *Phys. Rev. Lett.* **85**, 74 (2000).
- [41] T. Lu, H. Lee, T. Chen, S. Herchak, J.-H. Kim, S. E. Fraser, R. C. Flagan, and K. Vahala, *Proc. Natl. Acad. Sci. U. S. A.* **108**, 5976 (2011).
- [42] W.-L. Jin, X. Yi, Y.-W. Hu, B.-B. Li, and Y.-F. Xiao, *Appl. Opt.* **52**, 155 (2013).
- [43] C. F. Bohren and D. R. Huffman, *Absorption and Scattering by a Sphere* (Wiley Online Library, New York, 1983).
- [44] L. Deych and V. Shuvayev, *Phys. Rev. A* **92**, 013842 (2015).
- [45] M. R. Foreman and F. Vollmer, *New J. Phys.* **15**, 83006 (2013).
- [46] M. R. Foreman, D. Keng, J. R. Lopez, S. Arnold *et al.*, *Opt. Lett.* **42**, 963 (2017).
- [47] T. M. Habashy, R. W. Groom, and B. R. Spies, *J. Geophys. Res.* **98**, 1759 (1993).
- [48] Y. Hu, L. Shao, S. Arnold, Y.-C. Liu, C.-Y. Ma, and Y.-F. Xiao, *Phys. Rev. A* **90**, 043847 (2014).